The 8th European Congress on Computational Methods in Applied Sciences and Engineering
ECCOMAS Congress 2022
5-–9 June 2022, Oslo, Norway

A MATERIAL INTERPOLATION TECHNIQUE BASED ON THE SIMPLEX POLYTOPE

Konstantinos I. Ypsilantis[1], Matthias G.R. Faes[3], Jan Ivens[2] and David Moens[1]

[1] Reliable and Robust Design Lab,
[2] Structural Composites and Alloys, Integrity and Nondestructive Testing Lab,
Katholieke Universiteit Leuven,
Campus De Nayer, Jan Pieter de Nayerlaan 5, 2860 Sint-Katelijne-Waver, Belgium,
e-mail: {konstantinos[dot]ypsilantis, jan[dot]ivens, david[dot]moens}[at]kuleuven[dot]be

[3] Chair for Reliability Engineering,
Technische Universität Dortmund,
Leonhard-Euler-Strasse 5, 44227 Dortmund, Germany,
e-mail: matthias[dot]faes[at]tu-dortmund[dot]de

Key words: Discrete Material Optimization, Tetrahedral FE Shape Functions, Simplex Polytope, Topology Optimization.

Abstract. The Discrete Material Optimization (DMO) and the Shape Function with Penalization (SFP) constitute the state-of-the-art material interpolation techniques for identifying from a list of pre-defined candidate materials the most suitable one(s) for the structural domain. The candidate materials are represented on this list through their mechanical properties, and are interpolated within the domain of interest (DOI), whether that is the finite element (FE) domain or groups of FEs, so-called patches. Depending on the technique preferred to interpolate the mechanical properties within the DOI, a different type of weights is selected. Goal of the discrete material optimization problem (MOP) is to solve for these weights and determine for each FE/patch a unique material from the list. The current work extends the concept of the SFP technique by employing as weights the shape functions of the hyper-tetrahedral FE, the dimension of which is dynamically adapted depending on the number of candidate materials considered for the structural domain. This generalized hyper-tetrahedral FE constitutes what is defined as a *simplex*, and similar to the SFP technique each of its nodes is tied to a specific candidate material. In the context of discrete optimization and utilizing the shape functions of an abstract high-dimensional FE as weights for the candidate materials, the proposed interpolation technique secures the continuity between the number of candidate materials that can be considered for the structure, a feature lacking in the SFP technique. Additionally, given that the number of nodes forming the simplex FE is always one unit greater than the dimension of the space it is defined within, the dimension of the resulting MOP drops by one per DOI. The developed material interpolation technique is combined with the topology optimization problem (TOP) to formulate the concurrent material and topology optimization problem for compliance minimization of the structure. Finally, the latter is examined on the academic case study of the 3D Messerchmitt-Bölkow-Blohm (MBB) beam for the case of the concurrent topology and discrete fiber orientation optimization problem.

1 INTRODUCTION

The deployment of composite materials has now become the norm for structures where the combination of high mechanical properties and low weight forms the primary requirement, with the main metric for comparing the various candidate composites being their specific properties. Exploiting their general orthotropy for optimizing and steering the orientation of the fiber towards the most intense load paths, constitutes the most widely studied topic in the field of discrete material optimization; the discrete material optimization problem (MOP) searches from a discrete list of pre-defined candidate materials that are considered for the structural domain, the most suitable one per DOI. Each of the candidate materials is represented on this list via their mechanical properties, and a parameterization scheme is implemented so as to interpolate the mechanical property within the DOI. Considering the case of n_c candidate materials assigned per FE (e) of the structural domain, discrete material optimization applies the following interpolation scheme:

$$[C_{e(\boldsymbol{w_e})}] = w_{e1} \cdot [C_1] + \cdots + w_{en_c} \cdot [C_{n_c}] = \sum_{i=1}^{n_c} w_{ei} \cdot [C_i], \tag{1}$$

where $w_{ei} \in [0, 1]$ is the weight assigned to the (i^{th}) in order candidate material from the list, and $[C_i]$ its elasticity tensor. Goal of the MOP is to solve for these weights and conclude at the end of the optimization procedure to a unique material for each FE. The latter requirement implies that the predicted solution must be binary, *i.e.*, $w^*_{ei} = \{0, 1\}$ under the constraint that $\sum_i w^*_{ei} = 1$. The w_{ei} weights vary depending on the technique selected to inteprolate the mechanical property within the DOI.

In the initial stage of the field, the state-of-the-art work in [1] set the basis for the variety of material interpolation techniques to follow, where the authors proposed the so-called discrete material optimization (DMO) technique. DMO comes in different variations, amongst which the DMO4 and DMO5 [2] stood out to be the most robust ones, and despite being the oldest interpolation technique, it still constitutes the go-to choice in most MOPs. However, its main computational shortcoming lies in having an equal number of design variables to the number of candidate materials considered for the DOI, increasing thus the dimension of the resulting MOP. In their attempt to tackle this issue, the shape function with penalization technique (SFP) was proposed in [3]-[4], where the authors introduced the shape functions of the 2^k-noded quadrangular FE, with $k \in \mathbb{N}^+$, as weights for the candidate materials. The idea behind this approach is that each candidate material is tied to a specific node on the quadrangular FE, and the solution is optimized with respect to the nodal coordinates configuration. Despite achieving a substantial reduction in the number of design variables in the MOP, SFP suffers from the constraint that the number of candidate material phases should be given in integer powers of base 2. As a generalization of the SFP technique, trying to bridge the gap between $[2^{k-1} + 1, 2^k]$ material phases, the bi-value coding parameterization method (BCP) was later proposed in [5]. In the framework of the continuous multi-material topology optimization problem, the normal distribution function was applied in [6] for selecting the optimal amongst different isotropic materials, an idea which was recently explored in [7] for the problem of continuous fiber angle optimization (CFAO), labeled as the Normal Distribution Fiber Optimization (NDFO) technique. The authors utilized the standard normal distribution as the weighting function for the candidate

fiber orientations, and illustrated that a unique design variable is needed per DOI regardless of the number of candidate materials assigned to it.

In the framework of the concurrent MOP and TOP [8], in [9] the authors proposed an extension of the DMO technique for the concurrent discrete material distribution and thickness optimization for laminated composites. The proposed methodology was extended in [10] by introducing the relative density as an additional design variable so as to effectively terminate individual plies throughout the laminate. With regards to the concurrent CFAO and TOP, the recent work in [11] is mentioned, where the authors examined the effect of the printing plane of the additive manufacturing (AM) process in the predicted topologies of the structural domain.

The present work is motivated by the SFP technique, where in the context of utilizing the shape functions of a FE as weights for the candidate materials, the shape functions of the $hyper-tetrahedral$ FE are employed. Here, the term $simplex$ defines the tetrahedral FE in any space $\mathbb{R}^k$, where $k \in \mathbb{N}^+$. As discussed in the upcoming sections, the advantage that comes with considering the shape functions of the hyper-tetrahedral FE is two-fold: (1_a) with respect to DMO, the dimension of the resulting MOP drops by one per DOI, $e.g.$, for the case where each FE is assigned a different material, the dimension of the resulting simplex-based MOP reduces by the number of FEs discretizing the domain compared to the corresponding DMO-based MOP, and (1_b) the summation equality constraint stated in Eq(1), is automatically satisfied due to the self-complementary property of the simplex's FE shape functions. (2) with respect to SFP, first order shape functions are employed for the interpolation scheme, and the continuity in the number of candidate materials is ensured, $i.e.$, they are longer restricted to integer powers of base 2.

The paper is structured as follows: in Sec.(2) the complete formulation of the concurrent simplex-based material and topology optimization problem for compliance minimization of the structure is presented, and in Sec.(3) the proposed interpolation scheme is demonstrated on the 3D MBB beam for the concurrent discrete fiber orientation and topology optimization problem.

2 FORMULATION OF THE CONCURRENT SIMPLEX-BASED DISCRETE MATERIAL AND TOPOLOGY OPTIMIZATION PROBLEM

In this section the concurrent discrete material and topology optimization problem is presented for compliance minimization of the structural domain. The two optimization problems are initially decoupled with the MOP being examined first, where the proposed technique for interpolating the properties of the candidate materials within the FE domain is presented. In a second step, the TOP is incorporated into the MOP by introducing the relative densities of the FEs discretizing the structural domain as additional design variables. More specifically, the section is organized as follows: since the proposed technique is based on utilizing the shape functions of the simplex as the weights cast on the different candidate materials, the definition of a simplex as a geometric shape is given in Sec.(2.1). In Sec.(2.2) the simplex is treated as a hyper-tetrahedral FE defined in $\mathbb{R}^k$, where $k \in \mathbb{N}^+$, whose shape functions are requested. In this context, and for purposes of more comprehensive understanding, their derivation process is elaborated through their geometric interpretation. Finally, in Sec.(2.3) the proposed interpolation scheme is derived and is then incorporated into the TOP to pose the final compliance minimization problem for the structural domain.

2.1 Definition of the simplex in the $\mathbb{R}^k$ space, where $k \in \mathbb{N}^+$

Following up on the concept of the SFP technique that the shape functions of a FE constitute the weights of the candidate materials, the shape functions of the $k-$dimensional tetrahedron are considered in this work. In this case, this generalized tetrahedron constitutes what is defined as a *simplex*: a simplex is the generalization of a non-zero volume tetrahedron to the $k-$dimensional space (simplest possible convex polytope), *e.g.* in two dimensions it is a triangle, in three dimensions a tetrahedron, in k dimensions a $(k+1)$-verticed hyper-tetrahedron. The direct consequence stemming from the definition of the simplex is that the number of its vertices is always by one greater the dimension of the space it is defined within *e.g.*, a simplex $\mathcal{F}$ defined in $\mathbb{R}^k$ is always formed by $(k+1)$ vertices.

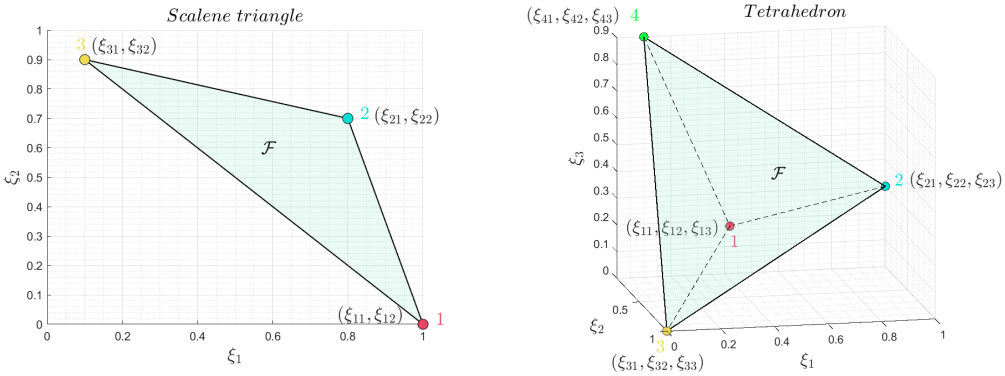

Figure 1: **(A)** The triangle is the simplex in $\mathbb{R}^2$. **(B)** The tetrahedron is the simplex in $\mathbb{R}^3$. Spanning $\mathbb{R}^3$, simplexes in higher dimensions are formed.

The volume of the simplex is explicitly defined by the coordinates of its vertices. Here, the notion of the volume is used in loose terms, since it loses its meaning for simplexes defined in any space other than $\mathbb{R}^3$. Specifically, for the triangle it contracts to the area of the triangle while for higher dimensional simplexes it is extrapolated to describe what is defined as a hyper-volume. The formula for calculating the volume of the simplex in $\mathbb{R}^2$, $\mathbb{R}^3$ and in higher dimensional spaces $\mathbb{R}^{k>3}$ is provided in Table 1. Here, each row of the matrix corresponds to a vertex of the simplex, and counting from the second column forth, each column contains the coordinates of the corresponding vertex in each direction (the first column is by default prepended to the matrix forcing it to be square).

A_0 in $\mathbb{R}^2$	V_0 in $\mathbb{R}^3$	V_0^k in $\mathbb{R}^k,\ k>3$
$\frac{1}{2!} \cdot abs\left(det \begin{bmatrix} 1 & \xi_{11} & \xi_{12} \\ 1 & \xi_{21} & \xi_{22} \\ 1 & \xi_{31} & \xi_{32} \end{bmatrix} \right)$	$\frac{1}{3!} \cdot abs\left(det \begin{bmatrix} 1 & \xi_{11} & \xi_{12} & \xi_{13} \\ 1 & \xi_{21} & \xi_{22} & \xi_{23} \\ 1 & \xi_{31} & \xi_{32} & \xi_{33} \\ 1 & \xi_{41} & \xi_{42} & \xi_{43} \end{bmatrix} \right)$	$\frac{1}{k!} \cdot abs\left(det \begin{bmatrix} 1 & \xi_{11} & \xi_{12} & \cdots & \xi_{1k} \\ 1 & \xi_{21} & \xi_{22} & \cdots & \xi_{2k} \\ \vdots & \vdots & \vdots & \ddots & \vdots \\ 1 & \xi_{(k+1)1} & \xi_{(k+1)2} & \cdots & \xi_{(k+1)k} \end{bmatrix} \right)$

Table 1: The formula for calculating the volume of the simplex in any given space.

2.2 Derivation of the simplex FE's shape functions

Let $\mathbb{R}^k$ be the space the simplex $\mathcal{F}_k$ is defined within. By definition, the corresponding simplex is constructed by $(k+1)$ vertices. Here, the terms "node" and "vertex" are interchangeable. The shape function associated with its (i^{th}) node $N_{i(\xi_1,\cdots,\xi_k)}$, is defined as the ratio of the volume of the hyper-tetrahedron formed by an internal point $P_{(\xi_1,\cdots,\xi_k)} \in \mathcal{F}_k$ with the rest of its vertices, $V_{i(\xi_1,\cdots,\xi_k)}$, to its total volume V_0. In mathematical terms, the above statement reads as follows:

$$N_{i(\xi_1,\cdots,\xi_k)} = \frac{V_{i(\xi_1,\cdots,\xi_k)}}{V_0} \in [0,1], \quad with \quad i \in \mathcal{V} = \{1,2,\cdots,k+1\}, \tag{2}$$

where, $\boldsymbol{\xi} = [\xi_1,\cdots\ \xi_k]$ are the coordinates of the internal point P. The calculation of the two volumes is carried out based on the formulas listed in Table 1; the calculation of V_0 yields a constant value -the volume of the simplex FE- while the volume V_i is parametrized by the coordinates of the internal point P. To calculate the latter, the coordinates of the (i^{th}) node ξ_{ij} with $j = 1:k$, are replaced by the coordinates of the point P in the matrix. As a general rule, the coordinates of the node whose shape function is sought are replaced by the coordinates of the internal point P in the matrix. For instance, expanding Eq.(2) for the case of the triangular FE, the shape function corresponding to the #1 node is written as follows:

$$N_{1(\xi_1,\xi_2)} = \frac{A_{1(\xi_1,\xi_2)}}{A_0} = \frac{\frac{1}{2!}\cdot abs\left(det\begin{bmatrix}1 & \xi_1 & \xi_2\\ 1 & \xi_{21} & \xi_{22}\\ 1 & \xi_{31} & \xi_{32}\end{bmatrix}\right)}{\frac{1}{2!}\cdot abs\left(det\begin{bmatrix}1 & \xi_{11} & \xi_{12}\\ 1 & \xi_{21} & \xi_{22}\\ 1 & \xi_{31} & \xi_{32}\end{bmatrix}\right)} \in [0,1] \tag{3}$$

where, $A_{1(\xi_1,\xi_2)}$ is the area of the triangle formed by the $(\#2,\#3)$ nodes and the internal point $P_{(\xi_1,\xi_2)}$, and A_0 the total area of the triangle. Figure $2_{(A)}$ illustrates the geometric interpretation of the shape functions for the triangular FE.

With regards to the tetrahedral FE, the shape function associated with the #1 node is expressed as follows:

$$N_{1(\xi_1,\xi_2,\xi_3)} = \frac{V_{1(\xi_1,\xi_2,\xi_3)}}{V_0} = \frac{\frac{1}{3!}\cdot abs\left(det\begin{bmatrix}1 & \xi_1 & \xi_2 & \xi_3\\ 1 & \xi_{21} & \xi_{22} & \xi_{23}\\ 1 & \xi_{31} & \xi_{32} & \xi_{33}\\ 1 & \xi_{41} & \xi_{42} & \xi_{43}\end{bmatrix}\right)}{\frac{1}{3!}\cdot abs\left(det\begin{bmatrix}1 & \xi_{11} & \xi_{12} & \xi_{13}\\ 1 & \xi_{21} & \xi_{22} & \xi_{23}\\ 1 & \xi_{31} & \xi_{32} & \xi_{33}\\ 1 & \xi_{41} & \xi_{42} & \xi_{43}\end{bmatrix}\right)} \in [0,1] \tag{4}$$

where, $V_{1(\xi_1,\xi_2,\xi_3)}$ the volume formed by the $(\#2,\#3,\#4)$ nodes and the internal point $P_{(\xi_1,\xi_2,\xi_3)}$, and V_0 the total volume of the tetrahedral FE. Figure $2_{(B)}$ illustrates the geometric interpretation of the shape functions for the tetrahedral FE.

Applying the same approach, the shape function tied to the #1 node of the hyper-tetrahedral FE is calculated. By cyclical alternation of the indices, the shape functions of the rest of the nodes are calculated.

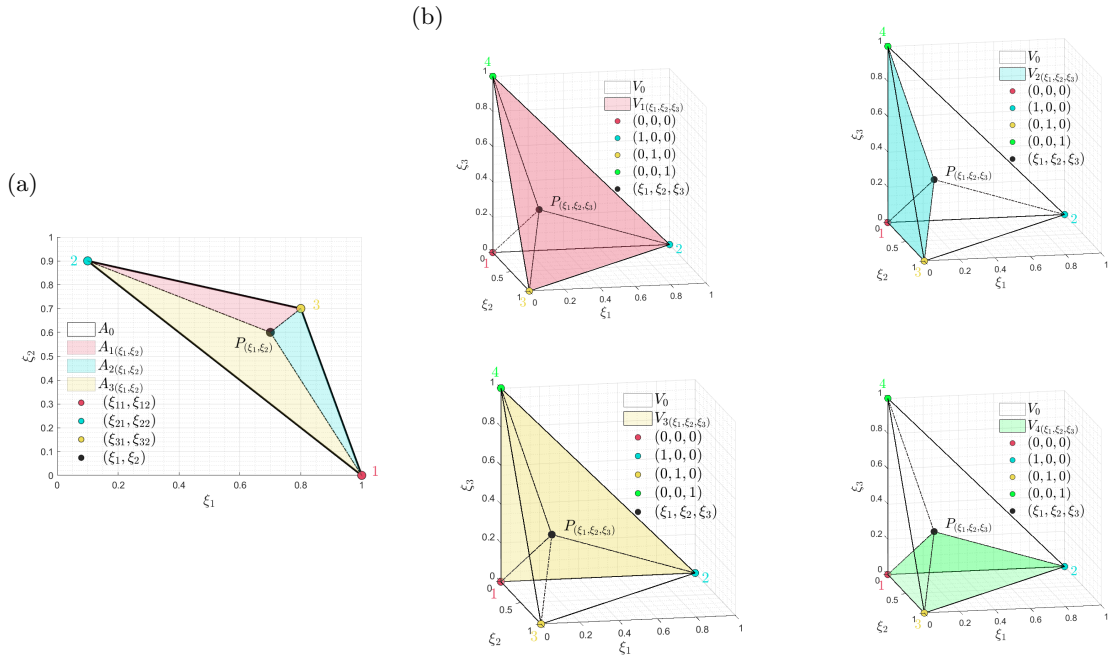

Figure 2: Geometric interpretation of the simplex FE's shape functions: (a) The shape function associated with each node of the triangular FE equals to the ratio of the area formed by the rest two nodes and the internal point $P_{(\xi_1,\xi_2)}$. (b) The shape function associated with each node of the unitary orthogonal tetrahedral FE equals to the ratio of the volume formed by the rest three nodes and the internal point $P_{(\xi_1,\xi_2,\xi_3)}$.

Given the freedom of considering different simplexes within a given space, for consistency purposes, the proposed material interpolation technique is presented for the case when the unitary orthogonal simplex FE is considered. The motivation behind this selection is two-fold: (1) the simplified mathematical description of the specific simplex FE as a linear convex set, which constitutes the feasible domain for the solution $P_{(\boldsymbol{\xi})}$, and (2) the identification of the permissible bounds of the $P_{(\boldsymbol{\xi})}$ point to those of the relative density of each FE; that is, the resulting MOP and TOP will share the same side constraints in their design variables. As such, scale-related computational issues stemming from the imposed constraints can be avoided in the final optimization problem.

Thus, considering the first node of the simplex FE being located at the origin and the rest of its nodes at a unit distance from the origin spanning the $\mathbb{R}^k$ space, its shape functions take the form listed in Table 2. Here, the domain of the $(k+1)$-noded orthogonal tetrahedral FE in $\mathbb{R}^k$ results from the intersection of the $[0,1]^k$ hyper-cube -where its natural coordinate system is defined- with the hyper-plane $g_{(\xi_1,\cdots,\xi_k)} : \sum_{i=1}^{k} \xi_i - 1 = 0$, expressed in the table in a L_1 norm format. The hyper-plane defines mathematically the hypotenuse of the simplex FE, as illustrated in Figure 3 for the cases of the orthogonal triangular and tetrahedral FEs, respectively.

#Node	$\mathcal{F}_2 = \{\boldsymbol{\xi} \in \mathbb{R}^2 \mid 0 \leq \boldsymbol{\xi} \leq 1, \|\boldsymbol{\xi}\|_1 - 1 \leq 0\}$	$\mathcal{F}_3 = \{\boldsymbol{\xi} \in \mathbb{R}^3 \mid 0 \leq \boldsymbol{\xi} \leq 1, \|\boldsymbol{\xi}\|_1 - 1 \leq 0\}$	$\mathcal{F}_k = \{\boldsymbol{\xi} \in \mathbb{R}^k \mid 0 \leq \boldsymbol{\xi} \leq 1, \|\boldsymbol{\xi}\|_1 - 1 \leq 0\}$
1	$\mathrm{N}_{1(\xi_1,\xi_2)} = 1 - \xi_1 - \xi_2$	$\mathrm{N}_{1(\xi_1,\xi_2,\xi_3)} = 1 - \xi_1 - \xi_2 - \xi_3$	$\mathrm{N}_{1(\xi_1,\cdots,\xi_k)} = 1 - \sum_{i=1}^{k} \xi_i$
2	$\mathrm{N}_{2(\xi_1,\xi_2)} = \xi_1$	$\mathrm{N}_{2(\xi_1,\xi_2,\xi_3)} = \xi_1$	$\mathrm{N}_{2(\xi_1,\cdots,\xi_k)} = \xi_1$
3	$\mathrm{N}_{3(\xi_1,\xi_2)} = \xi_2$	$\mathrm{N}_{3(\xi_1,\xi_2,\xi_3)} = \xi_2$	$\mathrm{N}_{3(\xi_1,\cdots,\xi_k)} = \xi_2$
4		$\mathrm{N}_{4(\xi_1,\xi_2,\xi_3)} = \xi_3$	$\mathrm{N}_{4(\xi_1,\cdots,\xi_k)} = \xi_3$
k+1			$\mathrm{N}_{k+1(\xi_1,\cdots,\xi_k)} = \xi_k$

Table 2: The shape functions of the unitary orthogonal simplex FE $\mathcal{F}_k$ in $\mathbb{R}^k$, $k \in \mathbb{N}^+$.

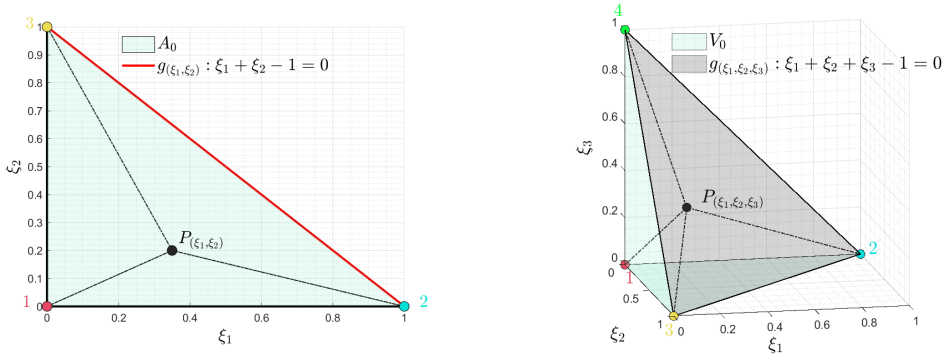

Figure 3: Depiction of (a) orthogonal triangular FE ($\mathcal{F}_2$), (b) orthogonal tetrahedral FE ($\mathcal{F}_3$).

2.2.1 The simplex-based material interpolation technique

Similar to the SFP technique each candidate elasticity tensor occupies a specific nodal location on the simplex FE. The goal of the resulting MOP is to optimize the objective function with respect to the coordinates of the internal point $P_{(\boldsymbol{\xi})}$. The dimension of the space the simplex is defined within, is dynamically adapted depending on the number of candidate materials considered for the structural domain. For instance, when considering n_c candidate materials for the structural domain, a n_c-noded unitary orthogonal tetrahedral FE is generated within the $\mathbb{R}^{n_c-1}$ space. Deploying the shape functions of the unitary orthogonal tetrahedral FE, listed in Table 2, to interpolate the n_c candidate materials within the (e^{th}) FE, the interpolated property reads as follows:

$$[C_{e(\boldsymbol{\xi_e})}] = \sum_{i=1}^{n_c} N_{ei(\boldsymbol{\xi_e})}^{p_n} \cdot [C_i], \tag{5}$$

where, $[C_i]$ the $[6 \times 6]$ elasticity tensor representing the (i^{th}) candidate material in the list, $N_{ei(\boldsymbol{\xi_e})}$ the corresponding (i^{th}) in order shape function of the simplex FE, and $p_n \in \mathbb{R}^+$ a penalty factor forcing the solution $P_{(\boldsymbol{\xi_e})}$ towards the location of the simplex's nodes. Notice that, for values of $p_n \neq 1$, an additional constraint must be imposed so that to enforce the self-complementary property on the shape functions within the simplex FE's domain, *i.e.*, $\sum_{i=1}^{n_c} N_{ei(\boldsymbol{\xi_e})}^{p_n} = 1$. Finally, the introduction of the subscript e in the shape functions, indicates that a different solution is

expected/enforced per FE (e), unless groups of FEs are assigned the same simplex FE to interpolate the candidate materials. Figure $4_{(A)}$ depicts the idea behind assigning the candidate materials to the nodes of the simplex FE. Figure $4_{(B)}$ depicts the final volume and shape function' values corresponding to the nodes of the simplex FE for the ideal case when a unique material is predicted at the end of the material optimization loop for the (e) FE.

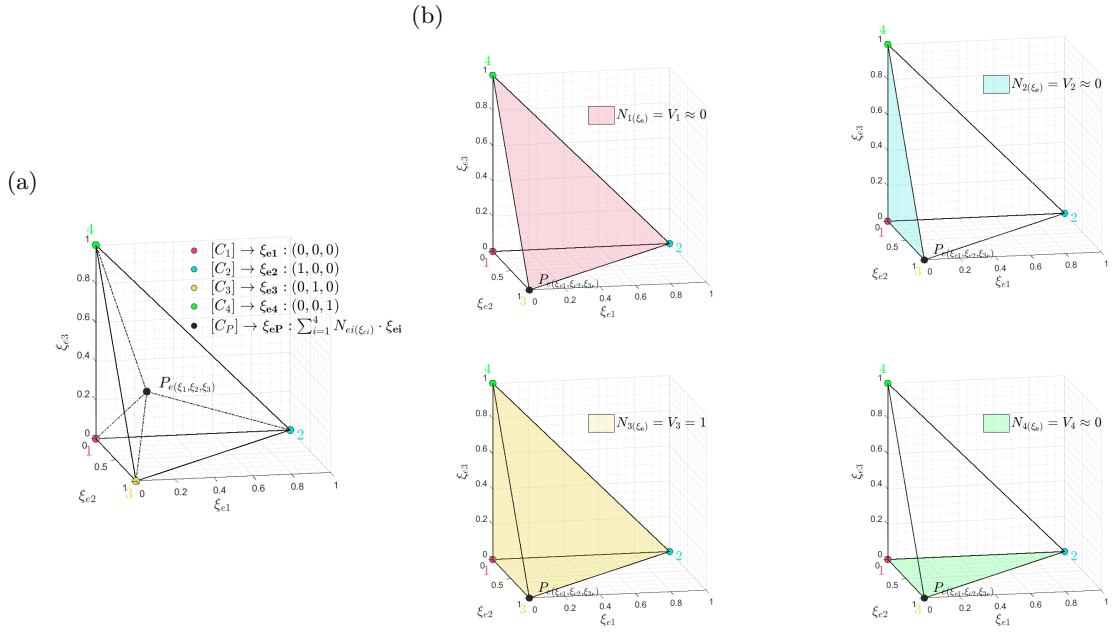

Figure 4: (a) Each candidate material is assigned to a nodal location on the tetrahedral FE. (b) For the case where the material #3 is predicted for the (e) element, the shape function of the #3 node equals to 1 and 0 for the rest.

Finally, the TOP is combined with the MOP by assigning per FE (e) in the structural domain a relative density x_e. As such, Eq.(5) is re-expressed as follows:

$$[C_{e(x_e,\boldsymbol{\xi_e})}] = x_e^p \cdot \Big(\sum_{i=1}^{n_c} N_{ei(\boldsymbol{\xi_e})}^{p_n} \cdot [C_i]\Big), \tag{6}$$

where $p \in \mathbb{R}^+$ a penalization factor forcing the intermediate relative density values towards to the $[10^{-3}, 1]$ bounds. For abbreviation purposes from now onwards, the $[x_e, \boldsymbol{\xi_e}]$ design variables associated with the (e) FE are grouped in a unique vector denoted as $\boldsymbol{dv_e} = [x_e, \boldsymbol{\xi_e}]$.

2.3 Formulation of the concurrent simplex-based material and topology optimization problem

In this section, the concurrent simplex-based material and topology optimization problem is posed for compliance minimization of the structure. In Sec.(2.3.1), the stiffness matrix is derived for the (e) FE, and in Sec.(2.3.2) the resulting compliance minimization problem is posed.

2.3.1 Derivation of the FE's stiffness matrix

Substituting the elasticity tensor derived in Eq.(6) into the volume integral calculating the stiffness tensor of the FE, the latter reads as follows:

$$[K_{e(\boldsymbol{dv_e})}] = x_e^p \cdot \left(\int_{V_E} [B_e]^T \cdot \Big(\sum_{i=1}^{n_c} N_{ei(\boldsymbol{\xi_e})}^{p_n} \cdot [C_i] \Big) \cdot [B_e] \; dV \right) =$$

$$x_e^p \cdot \left(\sum_{i=1}^{n_c} N_{ei(\boldsymbol{\xi_e})}^{p_n} \cdot \underbrace{\left(\int_{V_E} [B_e]^T \cdot [C_i] \cdot [B_e] \; dV \right)}_{[K_{ei}]} \right) = x_e^p \cdot \left(\sum_{i=1}^{n_c} N_{ei(\boldsymbol{\xi_e})}^{p_n} \cdot [K_{ei}] \right), \tag{7}$$

where, $[K_{ei}]$ is the $[24 \times 24]$ stiffness tensor corresponding to the (i^{th}) candidate material, V_E is the volume of the FE, and $[B_e]$ is the $[6 \times 24]$ Jacobian matrix of the FE's shape functions. It is noted that, unless penalized, the derivatives of the shape functions with respect to the $\boldsymbol{\xi_e}$ design variables yield a constant value, *i.e.* the Jacobian of the stiffness tensor is independent of the $\boldsymbol{\xi_e}$ design variables.

2.3.2 Posing the compliance minimization problem

The resulting compliance minimization problem is subjected to: (1) the system's equilibrium constraints of Eq.(9), (2) the volume constraint of Eq.(10), (3) the enforced self-complementary property constraint imposed on the penalized shape functions of Eq.(11), and (4) the side constraints of the design variables of Eq.(12):

$$\boldsymbol{dv}^* = \underset{\boldsymbol{dv} \in \mathbb{R}^{n_e \cdot n_c}}{\operatorname{argmin}} \; C_{(\boldsymbol{dv})} = \sum_{e=1}^{n_e} \{U_{e(\boldsymbol{dv_e})}\}^T \cdot [K_{e(\boldsymbol{dv_e})}] \cdot \{U_{e(\boldsymbol{dv_e})}\}, \tag{8}$$

s.t.

- $[K_{all(\boldsymbol{dv})}] \cdot \{U_{all(\boldsymbol{dv})}\} = \{F_{all}\} \Rightarrow \{H_{(\boldsymbol{dv})}\} \; : \Big(\sum_{e=1}^{n_e} [K_{e(\boldsymbol{dv_e})}] \cdot \{U_{e(\boldsymbol{dv_e})}\} \Big) - \{F_{all}\} = \{0\}, \tag{9}$

- $\dfrac{V_{t(\boldsymbol{x})}}{V_0} = f_{volfrac} \Rightarrow F_{(\boldsymbol{x})} : \dfrac{V_{t(\boldsymbol{x})}}{V_0 \cdot f_{volfrac}} - 1 = 0, \tag{10}$

- $h_{e(\boldsymbol{\xi}_e)} : \sum_{i=1}^{n_c} N_{ei(\boldsymbol{\xi}_e)}^{p_n} - 1 = 0, \quad with \quad e = 1 : n_e, \tag{11}$

- $g_{e(\boldsymbol{\xi_e})} : \|\boldsymbol{\xi_e}\|_1 - 1 \leq 0, \qquad$ - $\boldsymbol{dv_{e,min}} \leq \boldsymbol{dv_e} \leq \boldsymbol{dv_{e,max}}, \quad with \quad e = 1 : n_e, \tag{12}$

  $where, \qquad \boldsymbol{dv_{e,min}} = [10^{-3}, \underbrace{0, 0, \cdots, 0}_{[1 \times n_c - 1]}], \qquad \boldsymbol{dv_{e,max}} = [1, \underbrace{1, 1, \cdots, 1}_{[1 \times n_c - 1]}],$

where $\boldsymbol{dv} = \bigcup_{e=1}^{n_e} \boldsymbol{dv_e}$, $\boldsymbol{x} = \bigcup_{e=1}^{n_e} x_e$, n_e is the number of FEs discretizing the structural domain, $[K_{all(\boldsymbol{dv})}]$ is the global stiffness matrix, $\{U_{all(\boldsymbol{dv})}\}$ is the global displacement vector, $\{F_{all}\}$ is the external load vector (considered independent of the design variable vector $\boldsymbol{dv}$), $\{U_{e(\boldsymbol{dv_e})}\}$ is the displacement vector of the (e) element, $[K_{e(\boldsymbol{dv_e})}]$ its stiffness matrix, and $V_{t(\boldsymbol{x})}$ the final volume of the domain corresponding to the fraction $f_{volfrac}$ of its initial volume V_0.

3 NUMERICAL EXAMPLES

In this section the methodology is presented for the concurrent discrete fiber orientation and topology optimization problem. With regards to the former optimization problem, a list of predefined candidate fiber orientations is considered for the structure, amongst which the most optimal one is sought for each FE. Each candidate orientation is represented on the list via the corresponding effective mechanical property of the composite lamina, as derived by appropriately transforming it from the local to the global coordinate system (GCS). In the following examples, the engineering constants of the composite lamina are set equal to: $E_1 = 200\ GPa$, $E_2 = G_{12} = 20\ GPa$, $v_{12} = 0.3$, and $v_{23} = 0.3$. The composite lamina is considered to be specially orthotropic and transversely isotropic, with the latter implying that the rest of the engineering constants perpendicular to the lamina plane can be obtained by interchanging the subscripts 2 and 3 in the engineering constants.

The academic case study of the 3D MBB beam is examined in this section; the beam is simply supported at its lower two edges and a distributed load of $F = 100\ Nt$ is being applied in the middle of its lower face. The dimensions of the beam are $L_1 = 8\ m$, $L_2 = 4\ m$, and $L_3 = 0.01\ m$. With regards to the discrete fiber orientation optimization problem, the following list of candidate orientations is considered for the beam: $\Theta = \{0^0, -45^0, 45^0, 90^0\}$ about the X_3 axis of the GCS, as depicted in Figure 5; that is, the shape functions of the $4-$noded unitary orthogonal simplex FE are employed as weights for the candidate elasticity tensors. With regards to the TOP, 30% of the initial volume is selected to be kept, *i.e.*, $f_{volfrac} = 0.3$. For computational saving purposes, the p_n penalty factor is considered equal to unity, so that the self-complementary constraint of Eq.(11) is automatically satisfied, while the set of inequality constraints $g_{e(\boldsymbol{\xi_e})}$ of Eq.(12), holding for each FE in the domain, is aggregated into a scalar-valued global inequality constraint by means of the K-S function [12]. This transformation takes place as follows:

$$G_{(\boldsymbol{\Xi})} = \frac{1}{\eta} \cdot ln\Big\{ \sum_{e=1}^{n_e} e^{\eta \cdot g_{e(\boldsymbol{\xi_e})}} \Big\} - \frac{1}{\eta} \cdot ln(n_e) \tag{13}$$

where $\boldsymbol{\Xi} = \bigcup_{e=1}^{n_e} \boldsymbol{\xi}_e$, n_e the number of FEs, and $\eta \in [5, 200]$ a tunable parameter set equal to 50 in the test examples.

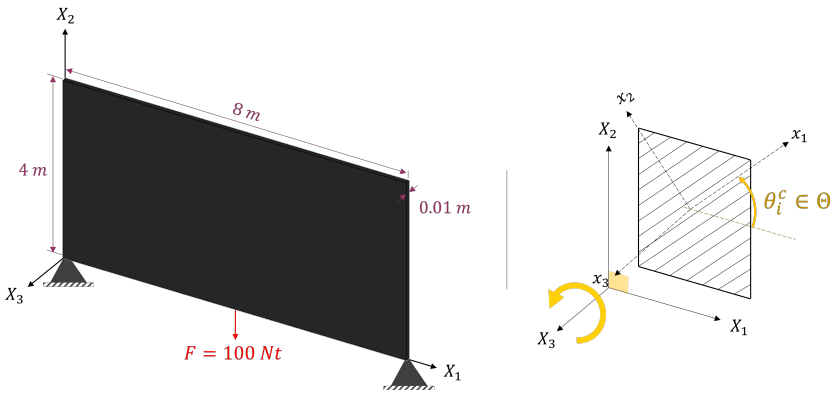

Figure 5: Depiction of the numerical example.

The numerical example is solved for two different mesh discretizations, a $[80 \times 40 \times 1]$ and a $[100 \times 50 \times 1]$ discretization mesh. The maximum number of iterations is set equal to $maxloop = 200$ and the prescribed tolerance between two successive iterations is set equal to $tol = 10^{-3}$. Finally, both optimization problems have been solved by means of the moving asymptotes solution algorithm (MMA) [13]. The predicted optimal topology and fiber orientation for both cases is presented in Figure 6, along with the convergence history in their compliance.

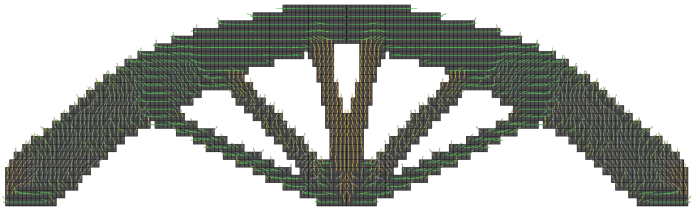

(a) **Mesh A**: $[80 \times 40 \times 1]$ Optimized domain and fiber distribution.

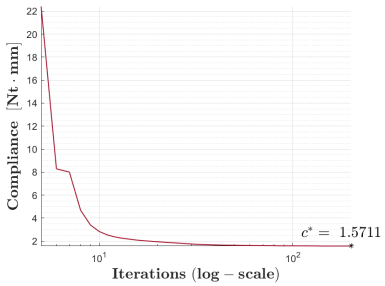

(b) The compliance history in semi-log scale.

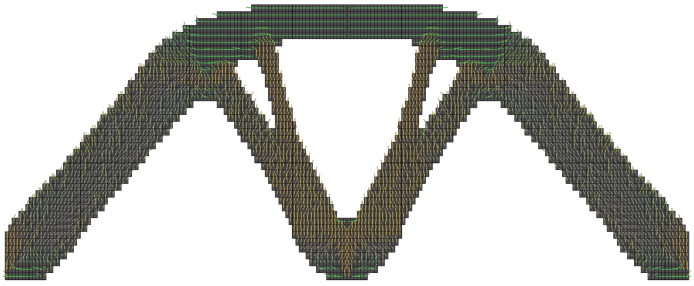

(c) **Mesh B**: $[100 \times 50 \times 1]$ Optimized domain and fiber distribution.

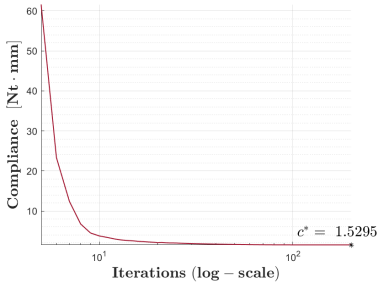

(d) The compliance history in semi-log scale.

Figure 6: The predicted results for the two mesh discretization cases of the MBB beam.

4 CONCLUSIONS

The scope of this work is to introduce a new material interpolation technique. Motivated by SFP, the proposed interpolation scheme utilizes the shape functions of the hyper-tetrahedral FE. The resulting concurrent discrete material and topology optimization problem is formulated for compliance minimization of the structural domain, and is demonstrated on the academic case study of the 3D MBB beam for the concurrent discrete fiber and topology optimization problem.

ACKNOWLEDGEMENTS

"Konstantinos Iason Ypsilantis acknowledges the support of the Research Foundation Flanders

(FWO) under the grant number 1SA8721N"

REFERENCES

[1] Stegmann, J. and Lund, E. *Discrete material optimization of general composite shell structures*. International Journal for Numerical Methods in Engineering (2005), **62**:2009-2027.

[2] Stegmann, J. *Analysis and optimization of laminated composite structures* (2004), Aalborg University.

[3] Bruyneel, M. *SFP– A new parameterization based on shape functions for optimal material selection: application to conventional composite plies* (2011), **43**:17-27.

[4] Bruyneel, M. and Duysinx, P. and Fleury, C. and Gao, T. *SFP: Extensions of the Shape Functions with Penalization (SFP) parameterization for composite plies optimization* (2011), **49**:979-1006.

[5] Gao, T. and Zhang, W. and Duysinx, P. *A bi-value coding parameterization scheme for the discrete optimal orientation design of the composite laminate*. International Journal for Numerical Methods in Engineering (2012), **91**:98-114.

[6] Yin L, Ananthasuresh GK. *Topology optimization of compliant mechanisms with multiple materials using a peak function material interpolation scheme*. Structural and Multidisciplinary Optimization (2001), **23**:49–62.

[7] Kiyono, C. Y., E. C. N. Silva, and J. N. Reddy *A novel fiber optimization method based on normal distribution function with continuously varying fiber path*. Composite Structures (2017), **160**:503–515.

[8] Bendsøe, M. P.*Optimal shape design as a material distribution problem*. Structural and Multidisciplinary Optimization (1989), **1**:193–202.

[9] Sørensen, S. N. and E. Lund. *Topology and thickness optimization of laminated composites including manufacturing constraints*. Structural and Multidisciplinary Optimization (2013), **48**:249–265.

[10] Sørensen SN, Sørensen R, Lund E. *DMTO—A method for discrete material and thickness optimization of laminated composite structures*. Structural and Multidisciplinary Optimization (2014), **50**:25–47.

[11] Jiang, Delin and Hoglund, Robert and Smith, Douglas E. *Continuous Fiber Angle Topology Optimization for Polymer Composite Deposition Additive Manufacturing Applications*. Fibers (2019), **7(2):14**.

[12] Wrenn, G. *An Indirect Method for Numerical Optimization Using the Kreisselmeier-Steinhauser Function*. NASA Contractor Report (1989).

[13] Svanberg, K. *The method of moving asymptotes - a new method for structural optimization.*International Journal for Numerical Methods in Engineering (1987), **(24)**:359–373.